arXiv:1603.06429v1 [nucl-th] 21 Mar 2016

Chapter 1

Foundations of Strangeness Nuclear Physics derived from chiral Effective Field Theory

Ulf-G. Meißner

HISKP and BCTP, Universität Bonn, D-53115 Bonn, Germany
IKP-3, IAS-4, JARA-HPC and JARA-FAME,
Forschungszentrum Jülich, D-52425 Jülich, Germany
meissner@hiskp.uni-bonn.de

Johann Haidenbauer

IKP-3 and IAS-4, Forschungszentrum Jülich, D-52425 Jülich, Germany
j.haidenbauer@fz-juelich.de

Dense compact objects like neutron stars or black holes have always been one of Gerry Brown's favorite research topics. This is closely related to the effects of strangeness in nuclear physics. Here, we review the chiral Effective Field Theory approach to interactions involving nucleons and hyperons, the possible existence of strange dibaryons, the fate of hyperons in nuclear matter and the present status of three-body forces involving hyperons and nucleons.

1. Introduction

Gerry Brown was a fascinating scholar and human being with a broad range of physics interests. One of his prime foci was the physics of dense and compact objects like neutron stars and black holes, see e.g. Refs.[1–8] With the observation of two solar mass neutron stars, this physics has taken a new twist, commonly referred to as the "hyperon puzzle". This puzzle relates to the fact that the equation of state in the presence of hyperons is generally too soft to allow for such heavy neutron stars. Some repulsive mechanism, may it be related to the hyperon-nucleon or hyperon-hyperon interactions, or even to more exotic three-body forces involving hyperons, is thus required to reconcile the presence of hyperons within such dense and compact objects with their global properties, see e.g. Refs.[9,10] (and

references therein). This is were some of our recent research comes in, namely the chiral Effective Field Theory (EFT) based description of the hyperon-nucleon (YN) in Sec. 2 and the hyperon-hyperon (YY) interactions in Sec. 3. Another related fascinating topic is the possible existence of exotic states with baryon number two, formed from two hyperons, which we will also discuss in Sec. 4. Next, we discuss the behavior of hyperons in nuclear matter in Sec. 5. Last but not least, we consider the final frontier, namely the three-body forces involving hyperons in Sec. 6. We are quite certain that Gerry would have loved these developments and we therefore dedicate this paper to his memory.

2. Hyperon-nucleon interactions

The basic ingredient in hyper-nuclear physics is the hyperon-nucleon interaction. Conventionally, it has been studied based on meson-exchange models, however, with the advent of successfull EFT methods for the nucleon-nucleon (NN) interaction (see Refs.[11,12] for reviews), one now has a better and more systematic handle on these fundamental interactions, firmly rooted in the symmetries of QCD. In contrast to the NN interaction, the amount of data on YN ($Y = \Lambda, \Sigma$) scattering is scarce, about 35 data points supplemented by the binding energies of a few light hyper-nuclei. Therefore, any EFT description of these data has a more exploratory character than it is the case for the NN problem. In fact, the first work on the YN interaction in EFT was due to Korpa et al.,[13] who made use of the so-called KSW power counting.[14] In the Bonn-Jülich group, we already had made good experiences with the so-called Weinberg power counting for the NN interactions. In that scheme, chiral perturbation theory is utilized for calculating the potential between two or more baryons in a systematic manner. This potential is then used within a regularized Lippmann-Schwinger (LS) equation to generate the bound and the scattering states, $T = V + VG_0T$, with T the T-matrix and G_0 the two-baryon propagator. The leading order (LO) $YN \to YN$ calculations were performed by Polinder and the authors[15] and later, the next-to-leading order (NLO) contributions were analyzed in collaboration with the Munich group of Norbert Kaiser, Stephan Petschauer and Wolfram Weise.[16] For a comparison of the EFT and more conventional approaches, see Ref.[17] In what follows, we eschew models.

The EFT is constructed from the asymptotically observed particles, the hadrons, here from the baryon octet (for short, baryons) and the Goldstone-boson octet (for short, mesons). The basic ingredient in the EFT approach

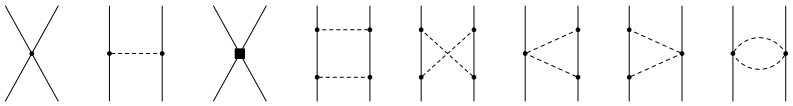

Fig. 1. Relevant diagrams for the effective potential up-to-and-including NLO. Solid and dashed lines denote baryons $(N, \Lambda, \Sigma, \Xi)$ and mesons (π, K, η), respectively. The square symbolizes a contact vertex with two derivatives. From left to right: LO contact term, one-meson exchange, NLO contact term, planar box, crossed box, left triangle, right triangle, football diagram. From the planar box graph, only the irreducible part contributes to the potential.

to the YN interaction is the effective potential, with its various terms ordered according to the power counting. At leading order, $\mathcal{O}(Q^0)$, where Q denotes an external momentum or a Goldstone boson mass, there are two types of contributions. First, one has one-meson-exchange graphs, with all couplings constants expressed in terms of the pion-nucleon coupling $g_{\pi NN}$ and the ratio of the SU(3) axial-couplings $F/(F+D)$. Second, based on group theory arguments, there are six four-baryon contact terms without derivatives. From those, only five contribute to the scattering process $YN \to YN$ while all six occur in the YY sector. Extending to NLO, one has now also contributions from two-meson-exchange diagrams and further contact interactions with two derivatives. The pertinent Feynamn diagrams are depicted in Fig. 1. All these have been calculated and included in the potential presented in Ref.[16] However, it should be stressed that some two-meson-exchanges like $K\bar{K}$ or ηK are so short-ranged that they could be also effectively absorbed in the contact terms. The number of additional contact interactions is large, so in general we resort to account only for SU(3) symmetric terms and fit only the low-energy constants (LECs) related to the S-wave terms and use P-wave NN phase shifts as constraints. However, physical masses of the mesons and the baryons are used throughout. This is needed to account properly for the fact that the pion mass is much smaller than that of the other Goldstone bosons and also to have the correct threshold energies for the various baryon-baryon channels, and it introduces a certain amount of SU(3) breaking.

In Fig. 2, we show some assorted results for the reactions $\Lambda p \to \Lambda p$ and $\Sigma^- p \to \Lambda n$. The middle panel zooms on the region around the $\Sigma^+ n$ and the $\Sigma^0 p$ thresholds for Λp scattering. In both cases, the bands at the given order are obtained by variations of the cut-off in the LS equation, that is applied in terms of the regulator function $f_R(\Lambda) = \exp[-(p'^4 + p^4)/\Lambda^4]$, with Λ the cut-off. This is only a very rough estimate of the theoretical

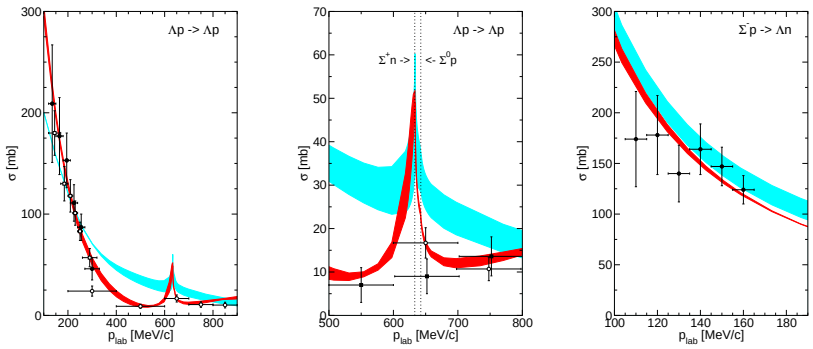

Fig. 2. Total cross section σ for $\Lambda p \to \Lambda p$ (left and middle panel) and for $\Sigma^- p \to \Lambda n$ (right panel) as a function of $p_{\rm lab}$. The red/dark band shows the chiral EFT results to NLO for variations of the cutoff in the range $\Lambda = 500 \ldots 650$ MeV, while the cyan/light band are results to LO for $\Lambda = 550 \ldots 700$ MeV. The data can be traced back from Ref.[16]

uncertainty and it should be revisited in the future upon the lines suggested e.g. in Refs.[18,19] However, we remark that the NLO contributions improve the description of the data and that the uncertainty bands shrink with increasing order.

3. Strangeness $S = -2, -3, -4$ baryon-baryon interactions

The experimental situation in the sector with strangeness $S = -2$ (YY and ΞN interactions), with $S = -3$ (ΞY interactions) and $S = -4$ ($\Xi\Xi$ interactions) is even poorer than for the hyperon-nucleon interaction. There are some constraints on the $\Lambda\Lambda$ interaction from double-Λ hyper-nuclei and from final-state interactions in production reactions. Similarly, there are bounds on the $\Xi^- p$ elastic cross section and for $\Xi^- p \to \Lambda\Lambda$ in a broad momentum range. There are some further results on in-medium cross sections and a few constraints from production experiments. For a detailed discussion, we refer the reader to Ref.[20]

It is therefore interesting to perform exploratory studies of the baryon-baryon interaction with $S = -2$ and with $S = -3, -4$ at LO, see Refs.[21,22] As already noted, at LO one has one more contact interaction in the $S = -2$ system compared to $S = -1$. Denoting the corresponding LEC by C_1 and varying its value within the natural range, given by[23] $|C_1| = 4\pi/F_\pi^2$, with F_π the pion decay constant, one observes that the chiral EFT predictions are consistent with the experimental information on the $S = -2$ sector.

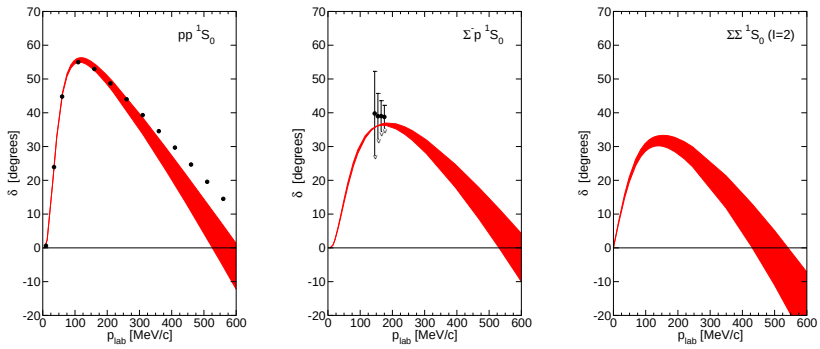

Fig. 3. pp, Σ^+p, and $\Sigma^+\Sigma^+$ phase shifts in the $^1S_0$ partial wave. The filled band represent the NLO result. The pp phase shifts of the GWU analysis[26] are shown by circles. In case of Σ^+p the circles indicate upper limits for the phase shifts, deduced from the Σ^+p cross section.

Using the LECs fixed in the fit to the ΛN and ΣN data, one can make predictions for the $\Xi\Lambda$, $\Xi\Sigma$ and $\Xi\Xi$ interactions. Strong attraction is found in some of the $S = -3$ and $S = -4$ channels, suggesting the possible existence of bound states. However, as we will argue below, these seem to be artefacts of the SU(3) symmetry imposed on the contact interactions.

In the approximation of taking only the SU(3) symmetric contact interactions, a consistent description of the NN and YN data is not possible. However, at NLO SU(3) breaking contact terms arise in the employed Weinberg power counting scheme.[24] These allow one to account for the leading SU(3) breaking terms in the $^1S_0$ wave for the baryon-baryon channels with maximal isospin, that contributes e.g. to nucleon-nucleon scattering via the potential $V_{NN}^{I=1} = C_1^\chi (M_K^2 - M_\pi^2)/2$, see Ref.[25] From a simultaneous description of the pp and the Σ^+p phase shifts one can pin down the LEC C_1^χ and then predict the $\Sigma\Sigma$ interaction, see Fig. 3. In the left panel of Fig. 4 we show the LO and NLO results for $\Xi^-p \to \Lambda\Lambda$ in comparison to the data from Ahn et al.[27] and Kim et al.[28] Both are consistent with these data. Note that the LO results are solely determined by the underlying SU(3) symmetry whereas in the NLO case the aforementioned SU(3) symmetry breaking in the $^1S_0$ wave is taken into account. The results for $\Xi^-p \to \Xi^-p$ shown in the right panel of Fig. 4 indicate that some degree of SU(3) symmetry breaking is also required in the $^3S_1$ partial wave. Specifically, we see that the inclusion of the leading SU(3) symmetry breaking term considerably lowers the prediction, giving a better agreement with the upper

bound from Ref.[27] (red/dark band). Relying strictly on SU(3) symmetry would yield cross sections that are apparently too large, cf. the hatched band. A more detailed account of these topics, including also discussions of the pertinent baryon-baryon scattering lengths and effective ranges can be found in Ref.[20] It is fairly obvious that to make further progress in this field, one needs more data, that are expected to come from the J-PARC facility in Japan and from FAIR at Darmstadt (Germany).

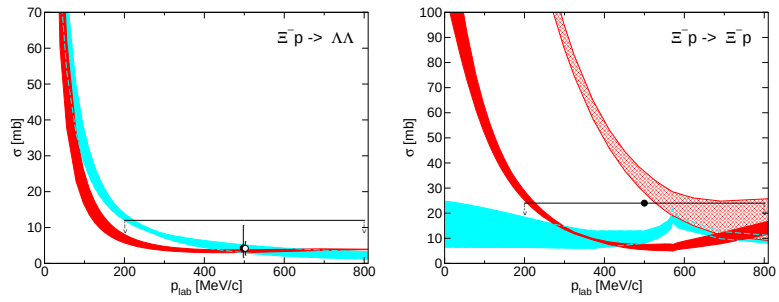

Fig. 4. Total cross section σ for $\Xi^- p \to \Lambda\Lambda$ (left panel) and for $\Xi^- p \to \Xi^- p$ (right panel) as a function of $p_{\rm lab}$. The red/dark band shows the chiral EFT results to NLO for variations of the cutoff in the range $\Lambda = 500 \ldots 650$ MeV, while the cyan/light band are results to LO for $\Lambda = 550 \ldots 700$ MeV. The hatched area in the right panel refers to a calculation where all LECs are taken over from the YN fit. The data can be traced back from Ref.[20]

4. Exotic bound states?

Another fascinating topic related to the baryon-baryon interactions is the possible appearance of (exotic) bound states. Historically, the so-called dibaryons have been conceived either as tightly bound six quark objects or as shallow bound states of two baryons. For the first category, the recently observed dibaryon $d^*(2380)$ at COSY (Forschungszentrum Jülich)[29,30] qualifies, whereas an established loosely bound state of a proton and the neutron, the deuteron, is one of the best studied nuclei. The deuteron is a bound state in the $^3S_1$-$^3D_1$ channel, whereas the binding of the proton-neutron system in the $^1S_0$ channel is just not strong enough to produce a bound state and only a virtual state is created. May be the most famous, – or should we say: infamous? – dibaryon is the H-particle predicted by Jaffe within the bag model as a compact $|uuddss\rangle$ state.[31] After decades of failed experiments to establish its presence, it regained popularity a few

years ago from lattice sightings reported in Refs.,[32,33] though at unphysical quark masses. The quantum numbers of the H are these of the $\Lambda\Lambda$ system in an S-wave state, namely strangeness $S = -2$, isospin $I = 0$, and $J^P = 0^+$. Other predicted dibaryons involving strangeness are cousins of the $d^*(2380)$[34] or generated from the attractive interaction between certain baryons, e.g. in the $\Xi\Xi$ but also for the $\Xi\Sigma$ and $\Xi\Lambda$ systems.[22,35] Note that the NPLQCD Collaboration reported evidence for a $\Xi^-\Xi^-$ bound state.[36] This list is by far not exhaustive but should merely serve as an illustration that there might be very rich physics in systems involving strangeness - strange exotics.

The chiral EFT discussed so far is very well suited to shed light on the H-dibaryon, should it indeed exist. In particular, one can study the implications of the imposed (approximate) SU(3) symmetry and further explore the dependence of its properties on the involved meson and baryon masses. The latter aspect is important as the existing lattice QCD calculations were not performed at the physical quark and thus hadron masses. In particular, one can use the flavor singlet LEC C_1 as a dial to generate a bound state with a given binding energy.[37,38]

The first issue to be discussed in this context is the effective range expansion in the ${}^1S_0$ channel of the $\Lambda\Lambda$ interaction. Let us assume that the H is a loosely bound two-baryon state much like the deuteron. For illustration, let us fix the value of the LEC C_1 such that the binding momentum of the H is the same as for the deuteron, $\gamma = 45.7\,\mathrm{MeV}$, related to the binding energy via $E = -\gamma^2/m_B$, with m_B either m_N or m_Λ. As it is well-known, the effective range expansion of Bethe and Schwinger relates the binding momentum to the scattering length a and effective range r, $1/a \simeq \gamma - r\gamma^2/2$. While this is very well fulfilled for the deuteron, the corresponding results for the $\Lambda\Lambda$-system in the ${}^1S_0$ wave are very different, $a \simeq -0.65\,\mathrm{fm}$ and $r \simeq 6\,\mathrm{fm}$.[20] Thus, the properties of the H are very different from the ones of the deuteron, despite the fact that both are close-to-threshold bound states. This can also be understood from the effective potentials in the $I = 0$ channel, the SU(3) flavor singlet $\sim C_1$ contributes with a much larger strength to ΞN than to $\Lambda\Lambda$. This means that the H should predominantly be a ΞN bound state. This can be sharpened by looking at the corresponding phase shifts, the one in the ΞN channel is rather similar to the NN ${}^3S_1$ phase shift, see Refs.,[37,38] see also Fig. 5.

Second, one can use the chiral EFT to vary the quark/pion mass to make contact to the lattice QCD results. If one sticks to the SU(3) symmetric case, one finds that for pion masses below 400 MeV, the dependence of

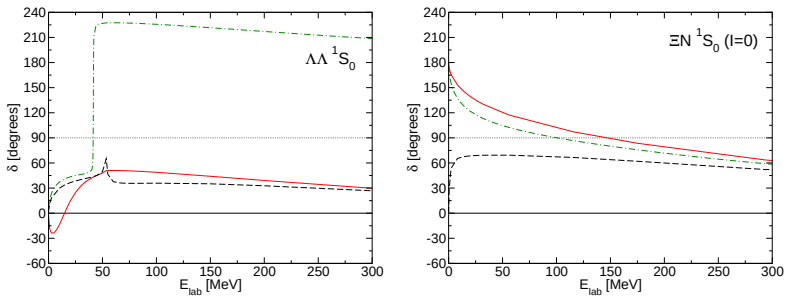

Fig. 5. Phase shifts for $\Lambda\Lambda$ ($^1S_0$) (left) and ΞN ($^1S_0$) (right) as a function of the pertinent laboratory energies. The solid line is the result for our reference BB interaction that produces a bound H at $E_H = -1.87$ MeV. The other curves are results for interactions that are fine-tuned to the H binding energies found in the lattice QCD calculations of the HAL QCD (dashed) and NPLQCD (dash-dotted) collaborations, respectively, for the pertinent meson (pion) and baryon masses as given by the lattice collaborations.

the binding energy of the H on M_π is linear, see also Ref.[39] In particular, if one adjusts the H binding energy to the value found by the NPLQCD collaboration at $M_\pi = 389\,\mathrm{MeV}$, it is reduced by 7 MeV when going to the physical point. For larger pion masses, this dependence is weakened but one should be aware that the EFT can not be trusted anymore at too large pion masses.

A third, and much more drastic effect, is caused by the SU(3) breaking related to the three thresholds for $\Lambda\Lambda$, $\Sigma\Sigma$ and ΞN, which are located at 2231.2, 2257.7, and 2385.0 MeV, in order. For physical values, the binding energy of the H is reduced by as much as 60 MeV as compared to an SU(3) symmetric interaction with degenerate two-baryon thresholds. For the lattice QCD results of the HAL QCD collaboration, this means that the bound state has disappeared at the physical point where as for the NPLQCD case, a resonance in the $\Lambda\Lambda$ system might survive, cf. also Fig. 5. The intricacies of coupled channel systems at unphysical quark masses are further discussed in the appendix.

As noted above, there have been speculations about bound states in two-baryon systems with $S = -3$ and $S = -4$, as e.g. given by the LO and NLO SU(3) symmetric interactions in our EFT. However, we have rexamined the role of SU(3) breaking in Ref.[25] As worked out by Kaiser and Petschauer,[24] there are 12 leading order symmetry breaking terms with corresponding LECs, from which 6 appear in the $^1S_0$ and 6 in the $^3S_1$ partial wave. At present, there is simply not enough information to determine these all. However, if we restrict ourselves to the BB systems

in the $^1S_0$ wave with maximal isospin, only two such LECs survive, called C_1^χ and C_2^χ. We had already discussed in Sec. 3 how to fix C_1^χ. The other LEC can not be pinned down reliably at present, but must be varied within a reasonable range. Including the symmetry breaking $\sim C_1^\chi$ in the $\Sigma\Sigma$ channel, the scattering length and the corresponding attraction is much reduced so that practically any bound state in this system can be ruled out. It is reasonable to assume that C_2^χ is of the same size as C_1^χ and that the increase in repulsion when going from NN to ΣN to $\Sigma\Sigma$ is not reversed for the $S=-3$ and $S=-4$ systems. In that case, bound states in these systems are also rather unlikey. For a more detailed discussion, we refer the reader to Ref.[25]

5. Hyperons in nuclear matter

Apart from the quest to find repulsion in the YN interaction, there are other interesting aspects of the behavior of hyperons in nuclei or nuclear matter. In particular, the repulsive nature of the Σ-nucleus potential[40] and the weak Λ-nucleus spin-orbit interaction[41–43] are long-standing issues, on which our calculations of hyperons in nuclear matter have shed some light.[44,45]

First, we consider the antisymmetric spin-orbit force. It is generated from the NLO potential $V \sim (\vec{\sigma}_1 - \vec{\sigma}_2)\cdot(\vec{q}\times\vec{k})$, in terms of the Pauli spin matrices, the exchange momentum $\vec{q}$ and the total momentum $\vec{k}$. This term gives rise to (spin) singlet-triplet ($^1P_1$-$^3P_1$) transitions. In our study of the YN interaction in free space[16] this antisymmetric spin-orbit force was set to zero because it can not be determined from YN scattering data. Matters are different in nuclei. Here, the strength of the spin-orbit interaction is frequently parameterized in terms of the so-called Scheerbaum factor S_Y,[46] which is related to the hyper-nuclear spin-orbit potential via $U_Y^{\ell s}(r) = -(\pi/2)S_Y(1/r)(d\rho(r)/dr)\vec{\ell}\cdot\vec{\sigma}$, with $\rho(r)$ the nucleon density distribution and $\vec{\ell}$ the single-particle orbital angular momentum operator. The EFT approach allows us to tune the LEC related to the $^1P_1$-$^3P_1$ transition to achieve a value of[44] $S_\Lambda = -3.7\,\mathrm{MeV\,fm}^5$, in accordance with phenomenological determinations that give S_Λ in the range -4.6 to $-3.0\,\mathrm{MeV\,fm}^5$.[47,48]

The standard method to calculate the properties of hyperons in a nuclear medium is Brueckner theory. The Brueckner reaction matrix (G-matrix) is determined from a solution of the Bethe-Goldstone equation, $G(\omega) = V + V[Q/(e(\omega)+i\epsilon)]G(\omega)$, with V the pertinent free-space potential, $e(\omega)$ the energy denominator depending on the starting energy ω, and Q is the (angle-averaged) Pauli operator. Medium effects are thus generated

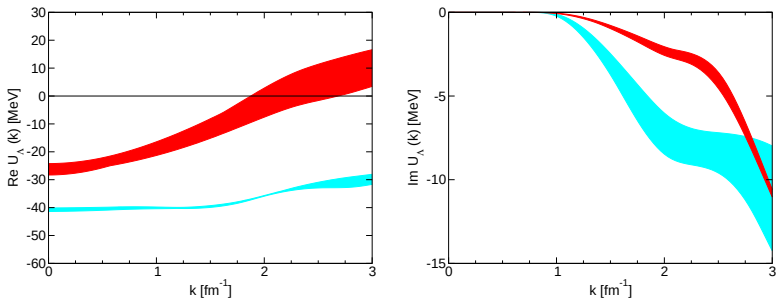

Fig. 6. Momentum dependence of the real and imaginary parts of the single-particle potential of a Λ hyperon in isospin symmetric nuclear matter at saturation density. The bands represent the variation of our results with the cutoff, see text.

from the Pauli operator as well as the density-dependent single-particle potential $U(\omega)$ in the energy denominator $e(\omega)$. This single-particle potential is obtained self-consistently from the G-matrix. There are two commonly used methods to calculate the G-matrix. In the so-called gap choice, only the free particle energies of the intermediate states appear in the energy denominator of the Bethe-Goldstone equation. This method was e.g. used in Ref.[44] In the so-called continuous choice, the dependence of the energy denominator on the full single-particle energies is retained. This method is computationally more difficult but allows to reliably access the imaginary parts of the single-particle potentials, which is not possible when the gap choice is employed. The results presented in Ref.[45] are based on the continuous choice.

In Fig. 6, we show the momentum dependence of the real and the imaginary part of the Λ single-particle potential in isospin-symmetric nuclear matter. The bands refer to the usual cut-off variations, using the continuous choice. We find $U_\Lambda(k=0) = -28 \ldots -24\,\mathrm{MeV}$, consistent with the empirical value of about $-28\,\mathrm{MeV}$ as deduced from binding energies of Λ hyper-nuclei.[49,50] The corresponding results for the neutral Σ in isospin-symmetric matter at saturation density are shown in Fig. 7, with small differences for the charged Σ hyperons given by the small inter-multiplet mass splittings. In pure neutron matter, matters are very different. Due to the maximal asymmetry between protons and neutrons, the single-particle potentials for the $\Sigma^+, \Sigma^0, \Sigma^-$ hyperons are rather different. These are discussed in detail in Ref.[45] As already said above, the resulting Λ-nuclear spin-orbit potential is small, which is partly due to cancellations between contributions from the symmetric and the anti-symmetric spin orbit forces,

and partly due to the repulsive interactions in some of the P-waves. The corresponding Scheerbaum factors for the Σ hyperons are much bigger than for the Λ. Specifically, for the neutral Σ we find $S_\Sigma = -15 \ldots -18\,\mathrm{MeV\,fm}^5$ at NLO. For more details, especially also a comparison between the results obtained in the gap and the continuous choice, see Refs.[44,45] Note that the in-medium hyperon spin-orbit interaction was also investigated in Refs.[47,51,52]

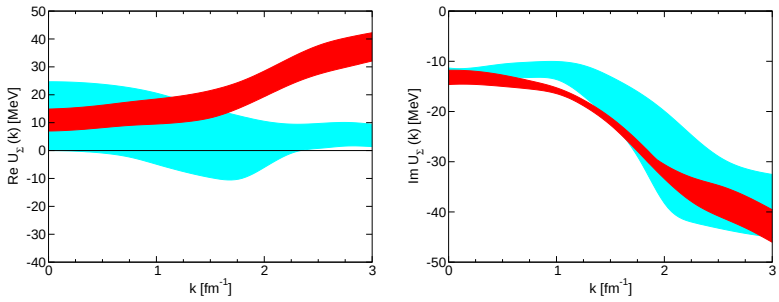

Fig. 7. Momentum dependence of the real and imaginary parts of the single-particle potential of a Σ^0 hyperon in isospin symmetric nuclear matter at saturation density. The bands represent the variation of our results with the cutoff, see text.

6. Three-baryon interactions

The need for (repulsive) three-baryon forces was already alluded to in the introduction. Another indication that points towards the necessity of such forces are the calculations of the binding energies of light hyper-nuclei at NLO by Nogga.[53] Here, the remaining cut-off dependence hints at missing three-body forces. More generally, it is well established that three-body forces are required in nuclei and nuclear matter, see e.g. Refs.[54,55]

In the Weinberg power counting, three-baryon forces (3BFs) appear at next-to-next-to-leading order and are given in terms of the three topologies shown in Fig. 8. The first and second topology require the meson-baryon Lagrangian at NLO. Its minimal form is given in Ref.[56] (see also Refs.[57,58]). The six-baryon contact terms given by the topology (3) require the general SU(3) Lagrangian that was constructed by Kaiser and Petschauer.[24] Armed with these ingredients, the leading three-baryon forces were derived in Ref.[59] within SU(3) chiral EFT. For that, the chiral Lagrangian in the non-relativistic limit with the minimal number of terms in the full SU(3)

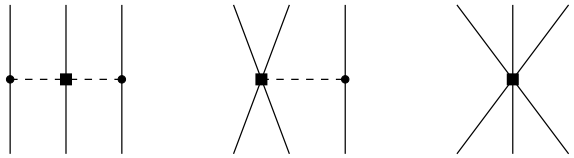

Fig. 8. Toplogies of the leading three-baryon forces. (1) Two-pion exchange terms, (2) one-pion exchange terms, and (3) six-baryon contact terms.

sector was derived. One finds that there are in total 18 different structures corresponding to topology (3) accompanied by 18 LECs. However, only a limited number of combinations of these LECs are involved in a given process. In general, one can write this local contribution to the 3BFs as

$$V^{\rm ct} = N_1 \mathbb{1} + N_2 \vec{\sigma}_1 \cdot \vec{\sigma}_2 + N_3 \vec{\sigma}_1 \cdot \vec{\sigma}_3 + N_4 \vec{\sigma}_2 \cdot \vec{\sigma}_3 + N_5 i \vec{\sigma}_1 \times \vec{\sigma}_2 \cdot \vec{\sigma}_3 \ , \quad (1)$$

in terms of the spin matrices of the three baryons and the N_i are prefactors containing LECs and kinematical factors, and we have suppressed the corresponding isospin factors, as detailed in Ref.[59] It can be shown that in the SU(2) limit one recovers the purely nucleonic contact term that is accompanied by the LEC E.[60] The graphs corresponding to the one-meson exchange topology (2) require the knowledge of combinations of the 14 four-baryon-one-meson vertices listed in Ref.[24] In spin-momentum space, this translates into the following structures:

$$V^{1\phi} = -\frac{1}{2F_\pi^2} \frac{\vec{\sigma}_1 \cdot \vec{q}_1}{\vec{q}_1^{\,2} + M_\phi^2} \Big\{ N_6 \vec{\sigma}_2 \cdot \vec{q}_1 + N_7 \vec{\sigma}_3 \cdot \vec{q}_1 + N_8 (\vec{\sigma}_2 \times \vec{\sigma}_3) \cdot \vec{q}_1 \Big\} \ , \quad (2)$$

where the N_i are again composed of LECs and kinematical factors. Further, $\vec{q}_i = \vec{p}_i\,' - \vec{p}_i$, with p_i and p_i' the initial and final momenta of baryon i, respectively. Again, in the SU(2) limit, one recovers the well-known term that is parameterized in terms of the LEC D, that can e.g. be determined from single pion production.[61] Finally, the diagrams corresponding to topology (1) are the generalizations of the well-known Fujita-Miyazawa three-nucleon force, when the decuplet is considered as very heavy. The spin-momentum structure of these terms takes the form

$$V^{2\phi} = -\frac{1}{4F_\pi^2} \frac{\vec{\sigma}_1 \cdot \vec{q}_1 \ \ \vec{\sigma}_3 \cdot \vec{q}_3}{(\vec{q}_1^{\,2} + M_{\phi_1}^2)(\vec{q}_3^{\,2} + M_{\phi_3}^2)} \times \Big\{ N_9 M_\pi^2 + N_{10} M_K^2 + N_{11} \vec{q}_1 \cdot \vec{q}_3 + N_{12} \vec{\sigma}_2 \cdot (\vec{q}_1 \times \vec{q}_3) \Big\} \ , \quad (3)$$

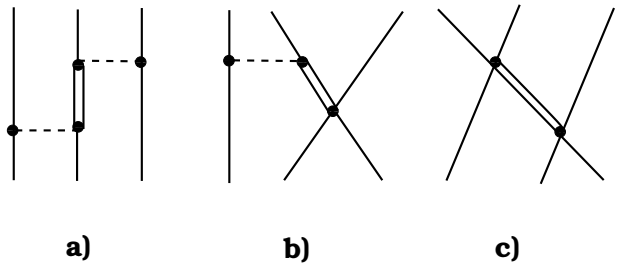

Fig. 9. Leading contributions to the three-baryon force at NLO in the theory with decuplet baryons. Solid, double and dashed lines denote octet baryons, decuplet baryons and Goldstone bosons, in order. The circles represent leading vertices. The diagram of type b) with a decuplet baryon in the initial state is not shown.

in the same notations as before. Again, in the SU(2) limit this expression recovers the well-known result in terms of the pion-nucleon LECs $c_{1,3,4}$, cf. e.g. Refs.[60,62] The complete expressions for the much thought after ΛNN three-body force can be found in Ref.[59]

At first sight, the large number of LECs (or combinations thereof) seems to be discomforting. It certainly is not possible to fix all these from data at present. However, one can use decuplet saturation for estimating these LECs. This is based on the successful resonance saturation hypothesis in the pion-nucleon sector[63] that has already been utilized to estimate nucleonic three-body forces in Refs.[62,64,65] For that, consider the theory with explicit decuplet degrees of freedom. Here, the three-body forces appear already at NLO, and the pertinent diagrams are shown in Fig. 9. These diagrams involve two kinds of vertices. First, there is the leading meson-baryon-baryon vertex with an octet baryon and a decuplet baryon (graphs (a) and (b)). The corresponding LEC $\mathcal{C}$ (sometimes also called h_A) can be estimated from the decay width $\Delta \to N\pi$, and one finds $\mathcal{C} = 3g_A/4 \simeq 1$, with g_A the nucleon axial-vector coupling constant. SU(3) symmetry can then be used to fix the values for all other possible combinations of octet and decuplet baryons. The other kind of vertices are the ones with three octet baryons and one decuplet baryon (appearing in graphs (b) and (c)). Those vertices involve two new constants. In this case the pertinent constants can not be deduced from considering the $3N$-Δ vertex simply because in leading order the latter is Pauli forbidden. That there are exactly two such terms can be easily understood from group theoretical considerations, for details see Ref.[66] Let us call the corresponding LECs G_1 and G_2 and consider the various topologies in detail and their behaviour in the limit of infinite decuplet masses, keeping the ratio

of coupling constants over decuplet mass fixed. The graph (a) is nothing but the dominant contribution to the famous Fujita-Miyazawa force. Its emergence in chiral EFT is discussed in detail in Ref.[67] In the heavy decuplet limit, this type of graphs generates the topology (1) of Fig. 8, with the LECs in the theory without decuplet given in very symbolic notation by $C^{2\phi} \sim \alpha_{2\phi}\mathcal{C}^2/\Delta$, where $\alpha_{2\phi}$ is some numerical factor and Δ denotes the decuplet-octet mass splitting. Similarly, the one-pion exchange topology (2) in the theory without the decuplet is generated from the terms of the type (b) in Fig. 9, leading to LECs with their strengths given by $C^{1\phi} \sim \alpha_{1\phi}\mathcal{C}(G_1 + \beta_{1\phi}G_2)/\Delta$, again with $\alpha_{1\phi}$ and $\beta_{1\phi}$ numerical factors. Finally, the graphs of the type (c) lead to local six-baryon contact interactions with their LECs given by $C^{\rm ct} \sim \alpha_{\rm ct}(G_1 + \beta_{\rm ct}G_2)^2/\Delta$. Explicit expressions for the ΛNN force can be found in Ref.[66] Eventually, these LECs might also be computed directly from lattice QCD, say along the lines of Ref.[68] We are looking forward to such calculations. To end this section, we stress that it will be of utmost interest to work out the consequences of these three-baryon forces within hyper-nuclei and compact dense objects like neutron stars.

Acknowledgements

We thank Tom Kuo and Ismail Zahed for inviting us to write this paper. We acknowledge fruitful collaborations with Norbert Kaiser, Andreas Nogga, Stefan Petschauer and Wolfram Weise. This work was supported in part by DFG and NSFC (CRC 110), by the HGF Virtual Institute NAVI (grant no. VH-VI-417) and by the Chinese Academy of Sciences (CAS) President's International Fellowship Initiative (PIFI) (Grant No. 2015VMA076).

A.1. Coupled channel dynamics on the lattice: Intricacies

Here, we briefly summarize the work of Ref.[69] that nicely exhibits the intricacies one faces when one is dealing with a coupled channel system at unphysical quark masses in a finite volume. The starting point is the observation, first made by the Munich group,[70] that the baryon resonance $S_{11}(1535)$ can be generated through coupled channel dynamics in the πN, ηN, $K\Lambda$ and $K\Sigma$ systems with total isopin $I = 1/2$ in the odd-parity S_{11} partial wave of pion-nucleon scattering. Including also NLO terms in the interaction kernel and using a field theoretical regularization method, this calculation was sharpened in Ref.,[71] where it was shown that also the next

resonance, the $S_{11}(1650)$, is generated dynamically, see also Ref.[72] for a similar conclusion.

In Ref.[69] we have considered two lattice set-ups that allow to investigate the rich phenomenology in the odd-parity S_{11} partial wave for varying quark masses. Set A is related to the work of the European Twisted Mass collaboration (ETMC). In this set-up the meson masses and pion decay constant are taken from the recent calculation in $N_f = 2 + 1 + 1$ twisted mass lattice QCD, i.e. ensemble $B25.32$ of Ref.[73] For the lattice size of $L/a = 32$ and spacing $a = 0.078$ fm, the pion mass is fixed there to $M_\pi = 269$ MeV, whereas the strange quark mass is held approximately at the physical value. As the kaon and eta decay constants are not available in this calculation at the moment, we decided to relate them to F_π with typical ratios of 1.15 and 1.3, respectively. The baryon masses are also taken from a calculation by the ETMC, however, with only two dynamical quarks and an older lattice action, see Ref.[74] Nevertheless, the strange quark mass is held again approximately at the physical value and $M_\pi = 269$ MeV for the identical lattice size and comparable lattice spacing, i.e. $a = 0.0855$ fm. The S_{11} amplitude, with the masses and decay constants of the ETMC, is shown in the left upper panel of Fig. A.1. Comparing to the physical situation, all thresholds have moved to higher energies. The cusp at the ηN threshold has become more pronounced, but no clear resonance shapes are visible. The structure of the amplitude becomes clearer by inspecting the complex energy plane on different Riemann sheets. This is visualized in the lower left panels of Fig. A.1. Compared to the physical point, the imaginary parts of the pole positions became much smaller due to the reduced phase space. Both the thresholds and the real parts of the pole positions have moved to higher energies. However, the thresholds have moved farther than the pole positions, such that the $N(1535)$ and $N(1650)$ poles are no longer situated below the part of the respective sheet, that is connected to the physical axis (thick horizontal lines). The poles are thus hidden and no clear resonance signals are visible in the physical amplitude. Instead, the amplitude is dominated by cusp effects.

Matters are very different for set B, that refers to calculation from QCDSF.[75] Here, baryon and meson masses are determined from an alternative approach to tune the quark masses, namely to start with the SU(3) symmetry limit and work at a fixed sum of the quark masses. Most importantly, while the lattice size and spacing are comparable to those of the ETMC, i.e. $L/a = 32$ and $a = 0.075$ fm, the strange quark mass differs significantly from the physical value. The latter results in a different order-

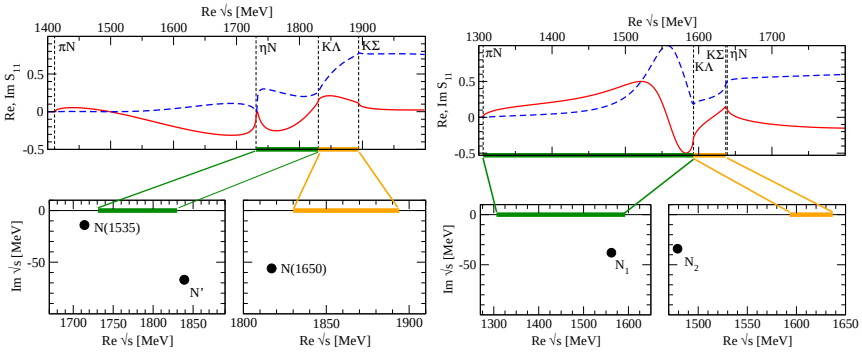

Fig. A.1. Left upper panel: Real (solid line) and imaginary part (dashed line) of the S_{11} amplitude, chirally extrapolated using masses and decay constants of the ETM collaboration. Left lower panels: two of the Riemann sheets with poles (left: Riemann sheet connected to the physical axis between the ηN and the $K\Lambda$ threshold. right: sheet connected to the physical axis between $K\Lambda$ and $K\Sigma$ threshold.). Right upper panel: Real (solid line) and imaginary part (dashed line) of the S_{11} amplitude, chirally extrapolated using masses and decay constants of the QCDSF collaboration.[75] Left lower panels: two of the Riemann sheets with poles (same as for ETMC).

ing of the masses of the ground-state octet mesons and, consequently, in a different ordering of meson-baryon thresholds. For further details we refer the interested reader to Ref.[75] The amplitude using the QCDSF parameter set is shown in the left upper panel of Fig. A.1. In contrast to the ETMC case, a clear resonance signal is visible below the $K\Lambda$ threshold, that is the first inelastic channel in this parameter setup. Indeed, we find a pole N_1 on the corresponding Riemann sheet, as indicated in the right lower first panel. Unlike in the ETMC case, it is not hidden behind a threshold. Between the $K\Lambda$ and the $K\Sigma$ threshold, there is only the hidden pole N_2 (right lower second panel). The $K\Sigma$ and ηN thresholds are almost degenerate and on sheets corresponding to these higher-lying thresholds we only find hidden poles.

This shows that the extraction of the scattering amplitude from lattice QCD data is a major challenge as we demonstrate by extrapolating the physical S_{11} amplitude of pion-nucleon scattering to the finite volume and unphysical quark masses, using a unitarized chiral framework including all next-to-leading order contact terms. As shown, the pole movement of the resonances $N(1535)1/2^-$ and $N(1650)1/2^-$ with varying quark masses is non-trivial. In addition, one can also calculate the finite volume energy levels. One finds that there are several strongly coupled S-wave thresholds that induce a similar avoided level crossing as narrow resonances. Consequently,

one has to be extremely careful in comparing lattice results at unphysical quark masses when a strong coupled channel dynamics is present. For more details, we refer the reader to Ref.[69] Finally, we note that pion-nucleon scattering in the negative parity channel in lattice QCD was considered by Lang and Verduci.[76]

References

1. O. Maxwell, G. E. Brown, D. K. Campbell, R. F. Dashen and J. T. Manassah, Astrophys. J. **216** (1977) 77.
2. G. E. Brown, K. Kubodera, D. Page and P. Pizzochero, Phys. Rev. D **37** (1988) 2042.
3. G. E. Brown and H. Bethe, Astrophys. J. **423** (1994) 659.
4. G. E. Brown, Nucl. Phys. A **574** (1994) 217C.
5. H. A. Bethe and G. E. Brown, Astrophys. J. **445** (1995) L129.
6. C. H. Lee, G. E. Brown and R. A. M. J. Wijers, Astrophys. J. **575** (2002) 996 [astro-ph/0109538].
7. A. Schwenk, B. Friman and G. E. Brown, Nucl. Phys. A **713** (2003) 191 [nucl-th/0207004].
8. C. H. Lee and G. E. Brown, J. Korean Phys. Soc. **49** (2006) S803 [astro-ph/0510380].
9. D. Chatterjee and I. Vidana, Eur. Phys. J. A **52** (2016) no.2, 29 [arXiv:1510.06306 [nucl-th]].
10. I. Bombaci, arXiv:1601.05339 [nucl-th].
11. E. Epelbaum, H. W. Hammer and U.-G. Meißner, Rev. Mod. Phys. **81** (2009) 1773 [arXiv:0811.1338 [nucl-th]].
12. R. Machleidt and D. R. Entem, Phys. Rept. **503** (2011) 1 [arXiv:1105.2919 [nucl-th]].
13. C. L. Korpa, A. E. L. Dieperink and R. G. E. Timmermans, Phys. Rev. C **65** (2002) 015208 [nucl-th/0109072].
14. D. B. Kaplan, M. J. Savage and M. B. Wise, Phys. Lett. B **424** (1998) 390 [nucl-th/9801034].
15. H. Polinder, J. Haidenbauer and U.-G. Meißner, Nucl. Phys. A **779** (2006) 244 [nucl-th/0605050].
16. J. Haidenbauer, S. Petschauer, N. Kaiser, U.-G. Meißner, A. Nogga and W. Weise, Nucl. Phys. A **915** (2013) 24 [arXiv:1304.5339 [nucl-th]].
17. J. Haidenbauer, U.-G. Meißner, A. Nogga and H. Polinder, Lect. Notes Phys. **724** (2007) 113 [nucl-th/0702015].
18. E. Epelbaum, H. Krebs and U.-G. Meißner, Eur. Phys. J. A **51** (2015) 53 [arXiv:1412.0142 [nucl-th]].
19. R. J. Furnstahl, N. Klco, D. R. Phillips and S. Wesolowski, Phys. Rev. C **92** (2015) 024005 [arXiv:1506.01343 [nucl-th]].
20. J. Haidenbauer, U.-G. Meißner and S. Petschauer, arXiv:1511.05859 [nucl-th].

21. H. Polinder, J. Haidenbauer and U.-G. Meißner, Phys. Lett. B **653** (2007) 29 [arXiv:0705.3753 [nucl-th]].
22. J. Haidenbauer and U.-G. Meißner, Phys. Lett. B **684** (2010) 275 [arXiv:0907.1395 [nucl-th]].
23. E. Epelbaum, Prog. Part. Nucl. Phys. **57** (2006) 654 [nucl-th/0509032].
24. S. Petschauer and N. Kaiser, Nucl. Phys. A **916** (2013) 1 [arXiv:1305.3427 [nucl-th]].
25. J. Haidenbauer, U.-G. Meißner and S. Petschauer, Eur. Phys. J. A **51** (2015) 17 [arXiv:1412.2991 [nucl-th]].
26. R.A. Arndt, W.J. Briscoe, I.I. Strakovsky and R.L. Workman, Phys. Rev. C **76** (2007) 025209; see also `http://gwdac.phys.gwu.edu/`
27. J. K. Ahn *et al.*, Phys. Lett. B **633** (2006) 214.
28. S. J. Kim, presentation at the *12th International Conference on Hypernuclear and Strange Particle Physics*, Sendai, Japan, 2015, see `http://lambda.phys.tohoku.ac.jp/hyp2015/`
29. P. Adlarson *et al.* [WASA-at-COSY Collaboration], Phys. Rev. Lett. **106** (2011) 242302 [arXiv:1104.0123 [nucl-ex]].
30. P. Adlarson *et al.* [WASA-at-COSY Collaboration], Phys. Rev. Lett. **112** (2014) 202301 [arXiv:1402.6844 [nucl-ex]].
31. R. L. Jaffe, Phys. Rev. Lett. **38** (1977) 195 [Phys. Rev. Lett. **38** (1977) 617].
32. S. R. Beane *et al.* [NPLQCD Collaboration], Phys. Rev. Lett. **106** (2011) 162001 [arXiv:1012.3812 [hep-lat]].
33. T. Inoue *et al.* [HAL QCD Collaboration], Phys. Rev. Lett. **106** (2011) 162002 [arXiv:1012.5928 [hep-lat]].
34. F. Dyson and N. H. Xuong, Phys. Rev. Lett. **13** (1964) 815.
35. V. G. J. Stoks and T. A. Rijken, Phys. Rev. C **59** (1999) 3009 [nucl-th/9901028].
36. S. R. Beane *et al.* [NPLQCD Collaboration], Phys. Rev. D **85** (2012) 054511 [arXiv:1109.2889 [hep-lat]].
37. J. Haidenbauer and U.-G. Meißner, Phys. Lett. B **706** (2011) 100 [arXiv:1109.3590 [hep-ph]].
38. J. Haidenbauer and U.-G. Meißner, Nucl. Phys. A **881** (2012) 44 [arXiv:1111.4069 [nucl-th]].
39. S. R. Beane *et al.*, Mod. Phys. Lett. A **26** (2011) 2587 [arXiv:1103.2821 [hep-lat]].
40. E. Friedman and A. Gal, Phys. Rept. **452** (2007) 89.
41. O. Hashimoto and H. Tamura, Prog. Part. Nucl. Phys. **57** (2006) 564.
42. A. Gal, Prog. Theor. Phys. Suppl. **186** (2010) 270.
43. E. Botta, T. Bressani and G. Garbarino, Eur. Phys. J. A **48** (2012) 41.
44. J. Haidenbauer and U.-G. Meißner, Nucl. Phys. A **936** (2015) 29 [arXiv:1411.3114 [nucl-th]].
45. S. Petschauer, J. Haidenbauer, N. Kaiser, U.-G. Meißner and W. Weise, Eur. Phys. J. A **52** (2016) 15 [arXiv:1507.08808 [nucl-th]].
46. R. R. Scheerbaum, Nucl. Phys. A **257** (1976) 77.
47. M. Kohno, Phys. Rev. C **81** (2010) 014003 [arXiv:0912.4330 [nucl-th]].
48. M. Kohno, *private communication*.

49. D. J. Millener, C. B. Dover, and A. Gal, Phys. Rev. C **38** (1988) 2700.
50. Y. Yamamoto, H. Bandō, and J. Zofka, Prog. Theor. Phys. **80** (1988) 757.
51. N. Kaiser and W. Weise, Nucl. Phys. A **804** (2008) 60 [arXiv:0802.1190 [nucl-th]].
52. N. Ishii *et al.* [HAL QCD Collaboration], PoS LATTICE **2013** (2014) 234; Eur. Phys. J. A **48** (2012) 41.
53. A. Nogga, Few Body Syst. **55** (2014) 757.
54. N. Kalantar-Nayestanaki, E. Epelbaum, J. G. Messchendorp and A. Nogga, Rept. Prog. Phys. **75** (2012) 016301 [arXiv:1108.1227 [nucl-th]].
55. H. W. Hammer, A. Nogga and A. Schwenk, Rev. Mod. Phys. **85** (2013) 197 [arXiv:1210.4273 [nucl-th]].
56. M. Frink and U.-G. Meißner, Eur. Phys. J. A **29** (2006) 255 [hep-ph/0609256].
57. A. Krause, Helv. Phys. Acta **63** (1990) 3.
58. J. A. Oller, M. Verbeni and J. Prades, hep-ph/0701096.
59. S. Petschauer, N. Kaiser, J. Haidenbauer, U.-G. Meißner and W. Weise, Phys. Rev. C **93** (2016) 014001 [arXiv:1511.02095 [nucl-th]].
60. E. Epelbaum, A. Nogga, W. Gloeckle, H. Kamada, U.-G. Meißner and H. Witala, Phys. Rev. C **66** (2002) 064001 [nucl-th/0208023].
61. C. Hanhart, U. van Kolck and G. A. Miller, Phys. Rev. Lett. **85** (2000) 2905 [nucl-th/0004033].
62. J. L. Friar, D. Huber and U. van Kolck, Phys. Rev. C **59** (1999) 53 [nucl-th/9809065].
63. V. Bernard, N. Kaiser and U.-G. Meißner, Nucl. Phys. A **615** (1997) 483 [hep-ph/9611253].
64. U. van Kolck, Phys. Rev. C **49** (1994) 2932.
65. E. Epelbaum, H. Krebs and U.-G. Meißner, Nucl. Phys. A **806** (2008) 65 [arXiv:0712.1969 [nucl-th]].
66. S. Petschauer, thesis, Technische Universität München (2015).
67. U.-G. Meißner, AIP Conf. Proc. **1011** (2008) 49.
68. S. R. Beane, W. Detmold, T. C. Luu, K. Orginos, M. J. Savage and A. Torok, Phys. Rev. Lett. **100** (2008) 082004 [arXiv:0710.1827 [hep-lat]].
69. M. Döring, M. Mai and U.-G. Meißner, Phys. Lett. B **722** (2013) 185 [arXiv:1302.4065 [hep-lat]].
70. N. Kaiser, P. B. Siegel and W. Weise, Phys. Lett. B **362** (1995) 23 [nucl-th/9507036].
71. P. C. Bruns, M. Mai and U.-G. Meißner, Phys. Lett. B **697** (2011) 254 [arXiv:1012.2233 [nucl-th]].
72. J. Nieves and E. Ruiz Arriola, Phys. Rev. D **64** (2001) 116008 [hep--ph/0104307].
73. K. Ottnad *et al.* [ETM Collaboration], JHEP **1211** (2012) 048 [arXiv:1206.6719 [hep-lat]].
74. C. Alexandrou *et al.* [ETM Collaboration], Phys. Rev. D **80** (2009) 114503 [arXiv:0910.2419 [hep-lat]].
75. W. Bietenholz *et al.*, Phys. Rev. D **84** (2011) 054509 [arXiv:1102.5300 [hep-lat]].
76. C. B. Lang and V. Verduci, Phys. Rev. D **87** (2013) 054502 [arXiv:1212.5055].